Title
Pressure-induced ion pairing in MgSO4 solutions: Implications for the oceans of icy worlds

Journal
Geochemical Perspectives Letters, 3(1)

ISSN
2410-339X

Authors
Schmidt, C
Manning, CE

Publication Date
2017

DOI
10.7185/geochemlet.1707

Peer reviewed

Geochemical Perspectives Letters

Pressure-induced ion pairing in $MgSO_4$ solutions: Implications for the oceans of icy worlds

C. Schmidt[1]*, C.E. Manning[2]

Abstract

At ambient temperature, liquid water transforms from a low-density to a high-density dynamic structure at ~0.2 GPa. The transition persists in electrolyte solutions; however, its effects on solute properties are unknown. We obtained Raman spectra of 0.5–2.0 molal $MgSO_4$ solutions at 21 °C and 10^{-4} to ~1.6 GPa. Above about 0.4 GPa, we observed an increase in the $MgSO_4$ contact ion pair abundance with pressure, regardless of concentration. This phenomenon contravenes the general rule that dissolved salts dissociate upon compression, and is likely caused by the structural collapse in the solvent with pressure due to increased hydrogen-bond breaking. Increasing ion association in high-pressure aqueous solutions implies that, at a given salinity, high-density water in deep, cold planetary oceans and pore waters will possess lower ionic strength and electric conductivity than previously thought. This behaviour will also lead to higher ocean salinity in the interiors of Pluto and the largest icy moons of Jupiter and Saturn, Ganymede, Callisto, and Titan, or in exoplanet water-worlds, through enhancement of submarine silicate weathering.

Received 13 June 2016 | Accepted 29 September 2016 | Published 18 October 2016

Introduction

The physical properties of liquid water at ambient temperature consistently display anomalous behaviour upon compression to densities of ~1.1 g cm^{-3}. These include *e.g.*, radial distribution functions from X-ray scattering (Okhulkov *et al.*, 1994) and neutron diffraction (Soper and Ricci, 2000), a distinct anomaly in the high-frequency sound velocity from inelastic X-ray scattering experiments (Krisch *et al.*, 2002), the Raman shift of the O–H stretching vibration (Kawamoto *et al.*, 2004), the sound velocity from Brillouin spectroscopy (Li *et al.*, 2005),

1. Deutsches GeoForschungsZentrum (GFZ), Section 4.3 Chemistry and Physics of Earth Materials, Telegrafenberg, 14473 Potsdam, Germany
* Corresponding author (email: Christian.Schmidt@gfz-potsdam.de)
2. Department of Earth, Planetary, and Space Sciences, University of California, Los Angeles, CA 90025-1567, USA

and the isothermal compressibility (Mirwald, 2005). The experiments indicate a transition from an open structure in low-density water (LDW) to a structure with a collapsed second coordination shell in high-density water (HDW) (Soper and Ricci, 2000). Based on femtosecond infrared pump-probe spectroscopy on a D_2O-H_2O mixture, the LDW-HDW transition is at ~0.25 GPa at 273 K and ~0.2 GPa at 298 K, but not observed at 363 K (Fanetti *et al.*, 2014).

Dissolved salts also disrupt the hydrogen-bonded dynamic H_2O structure due to formation of hydration shells around the ions. It is not clear if, and by how much, the structure outside the first hydration shell is affected (Marcus, 2009), but there is considerable evidence that the LDW-HDW transition persists in saline solutions even at fairly high solute concentrations (Mirwald, 2005; Schmidt, 2009; Valenti *et al.*, 2012). However, the effects of the transition on solute-solute interactions have not been investigated. Here, we studied the pressure-dependent variation in contact ion pairing in $MgSO_4$ solutions at 21 °C over a large range in pressure across the LDW-HDW transition until the sample solidified upon compression. We used $MgSO_4$ solutions because they are thought to be important components of planetary oceans (Zolotov and Shock, 2001) and because Raman scattering from the symmetric stretching vibration of sulphate (ν_1-SO_4^{2-}) provides direct information about the fraction of contact ion pairs.

Compression-Enhanced Contact Ion Pairing

At all conditions, the Raman band shape in the ν_1-SO_4^{2-} region was accurately described using two Gaussian + Lorentzian components (Fig. S-1a). The higher wavenumber component is assigned to contact ion pairs $Mg^{2+}SO_4^{2-}$(aq) (CIP), and the lower wavenumber component, here designated SO_4*, includes Raman-indistinguishable contributions from unassociated SO_4^{2-}(aq) ions, solvent-shared ion pairs $Mg^{2+}(OH_2)SO_4^{2-}$(aq) (SIP), and double solvent-separated ion pairs $Mg^{2+}(OH_2)_2SO_4^{2-}$(aq) (2SIP) (Rudolph *et al.*, 2003). Spectra in the O–H stretching region were recorded for the 2.0 molal solution. A three component model yielded good fits with internally consistent results for all spectra (Fig. S-1b). We assign the components C2 and C3 at ~3450 cm^{-1} and ~3580 cm^{-1} to ν_1 and ν_3 of H_2O monomers (*e.g.*, Walrafen, 1962). The component C1 at ~3280 cm^{-1} is assigned to O–H stretching vibrations of strongly hydrogen-bonded, polymerised water species because the relative intensity of this component correlates with the dependence of polymerisation on pressure and temperature (*e.g.*, Sahle *et al.*, 2013) and decreases with addition of salt (*e.g.*, Walrafen, 1962).

In our experiments at 21 ± 1 °C, we obtained data for the ν_1-SO_4^{2-} Raman shift of the SO_4* and CIP components (Figs. 1a and 1b), the abundance of contact ion pairs, as calculated from the relative integrated intensities of the CIP and SO_4* components (Fig. 1c), and the Raman shifts of the three band components in the O–H stretching region (Fig. 1d). At each studied concentration of 0.5, 1.7 and 2.0 molal $MgSO_4$, increasing pressure produces linear changes in the ν_1-SO_4^{2-} Raman shift of SO_4* of ~6 $cm^{-1}GPa^{-1}$ for the data to 0.17 GPa (Fig. 1a).

Above 0.7 GPa, the pressure dependence of that Raman shift is also linear and independent of composition, but the slope is shallower (~3 $cm^{-1}GPa^{-1}$). All data show systematic negative departures from linearity beginning at 0.17 GPa, which corresponds to the LDW-HDW transition (Fig. 1a) and agrees with a previous study on $NaSO_4$ solutions (Schmidt, 2009). Departures from linearity continue to ~0.6 GPa. Similar behaviour is observed in the Raman shift of the CIP component in the same pressure interval (Fig. 1b).

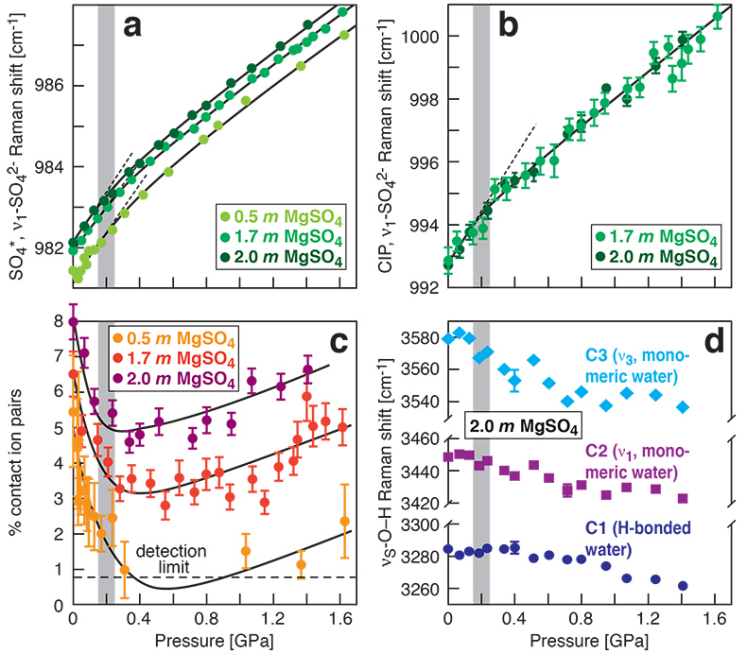

Figure 1 Raman spectroscopic results at 21 ± 1°C as a function of pressure. The shadowed band is the pressure range of the LDW-HDW transition at about 20°C (Fanetti *et al.*, 2014). **(a-b)** Raman shift ω of the ν_1-SO_4^{2-} mode of the SO_4* component (a) and of the CIP component (b). Dashed lines denote the $(\partial\omega/\partial P)_{T=21°C}$ slopes in $cm^{-1}GPa^{-1}$ from linear fits of data at <0.17 GPa. **(c)** Percentage of contact ion pairs as a function of pressure at 21°C. **(d)** Raman shift of fitted band components in the ν_S-O–H region of the 2.0 molal $MgSO_4$ solution.

At 21°C, the percentage of $Mg^{2+}SO_4^{2-}$(aq) CIP initially decreases with pressure along the isotherms at each concentration (Fig. 1c). Above ~0.4 GPa, however, it increases nearly linearly with rising pressure in 1.7 and 2.0 molal solutions. The 0.5 molal solution is consistent with this behaviour, although errors are larger and the abundance of CIPs is below the detection limit at about 0.4–0.9 GPa. This was not observed at 50–150°C, where the percentage of CIP in 0.75 and 2.25 molal $MgSO_4$ solutions generally decreased with pressure along all

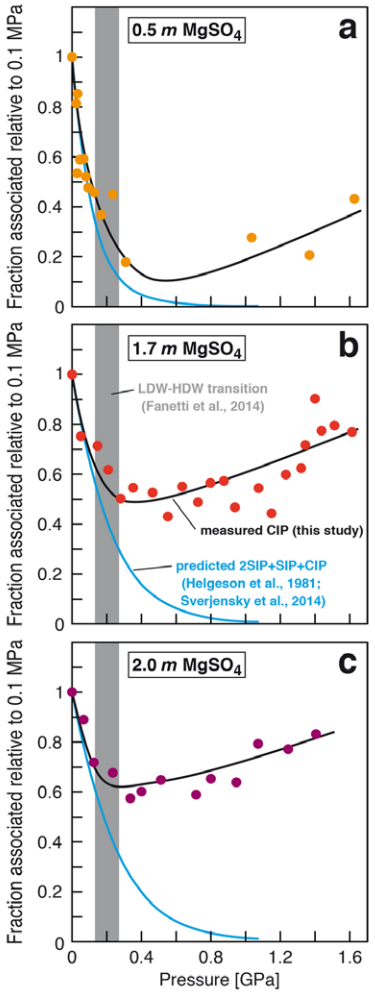

Figure 2 Fraction of $MgSO_4$ associated at 21 ± 1°C relative to that at ambient pressure, as determined by Raman spectroscopy and thermodynamic modelling, for 0.5 **(a)**, 1.7 **(b)**, and 2 molal solutions **(c)**. Thick black lines are trend lines for the fraction of CIP from Raman spectroscopic data fit by eye. Blue lines denote the fraction of the sum of the CIP, SIP and 2SIP ion pairs calculated from a thermodynamic model based on the DEW model (Sverjensky *et al.*, 2014) and the Helgeson-Kirkham-Flowers ion activity model (Helgeson *et al.*, 1981). The comparison assumes that the proportionality between equilibrium constants associated with expelling the H_2O molecules between ions is constant and independent of pressure. This assumption yields a minimum difference in predicted and observed CIP. The shadowed band is the pressure range of the LDW-HDW transition at about 20°C (Fanetti *et al.*, 2014).

isotherms (Fig. S-2). The data for the pressure dependence of the ν_S-O–H Raman shift for C1, C2 and C3 in the 2.0 molal solution generally suggest declining frequency with rising pressure (Fig. 1d), consistent with lengthening of the O–H-bonds and thus shorter hydrogen bonds between the water molecules. The scatter in these data is fairly large because the ν_S-O–H components are very broad and overlap (Fig. S-1b).

The finding of compression-enhanced contact ion pairing above ~0.2 GPa at 21 °C (Fig. 1c) is contrary to the predicted trend of increasing salt dissociation with pressure. Previous Raman spectroscopic and electrical conductivity studies (Ritzert and Franck, 1968; Chatterjee *et al.*, 1974) at less than about 0.5 GPa and near ambient temperatures indicated increasing dissociation of $MgSO_4$ in aqueous solution upon compression. Thermodynamic modelling also yields a continually increasing extent of ion pair dissociation with rising pressure, unaffected by the LDW-HDW transition (Fig. 2), but data used in such models are based on correlations and extrapolations typically derived from conductivity data at very different pressures and temperatures. The static dielectric constant of H_2O is a key parameter governing the extent of ion association in aqueous solutions; however, it does not decrease with increasing pressure in the HDW field (Fernandez *et al.*, 1995). Based on Coulomb's law, the observed increased contact ion pairing must therefore be caused by a decrease in the distance between cation and anion. An increasing tendency to form ion pairs with pressure can thus be related to increased hydrogen-bond breaking with pressure resulting in a collapsed second coordination shell in HDW (Soper and Ricci, 2000; Krisch *et al.*, 2002; Fanetti *et al.*, 2014). Therefore, the inferred relationship between water structure and ion pairing implies that significant interaction between ions and water exists at distances larger than the first shell, which has long been a matter of debate (*c.f.* Marcus, 2009).

Implications for Planetary Oceans and Interiors

Generally, the increase in ion pairing with pressure affects properties such as solubility, viscosity, sound absorption and electrical conductance. For a given salinity, isothermal salt re-association will yield lower ionic strength (and thus ion activity) than predicted from extrapolation of low-pressure behaviour, and also lower conductivity of deep ocean waters, which is relevant for the interpretation of spacecraft-based magnetometric data (*e.g.*, Hand and Chyba, 2007).

Our results show that high pressures and fairly low temperatures are required for pressure-induced ion pairing in salty water. In nature, it will therefore only occur in relatively large, cool planetary bodies with thick liquid water shells. Extrasolar ice planets may well meet these requirements, as well as some ocean planets such as Kepler-62e and -62f (Kaltenegger *et al.*, 2013). So too would cold, deep, aqueous planetary settings in our solar system, which include the interiors of Pluto and the largest icy moons of Jupiter and Saturn. There is considerable evidence for a subsurface ocean in Europa, but plausible basal ocean pressure is too low (Spohn and Schubert, 2003; Hand and Chyba, 2007) for salt

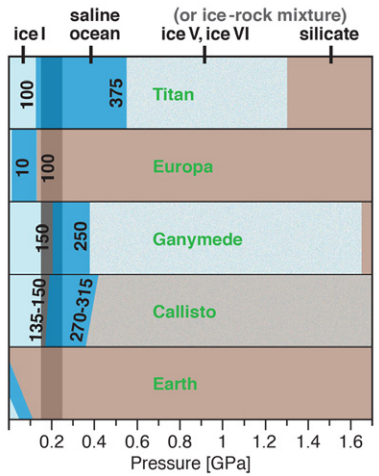

Figure 3 Comparison of models of the interiors of Titan (Tobie *et al.*, 2012), Europa (Spohn and Schubert, 2003; Hand and Chyba, 2007; Valenti *et al.*, 2012), Ganymede (Vance *et al.*, 2014; Saur *et al.*, 2015), and Callisto (Kuskov and Kronrod, 2005) with approximate depths of the subsurface ocean boundaries in km. The shadowed band is the pressure range of the LDW-HDW transition at about 20 °C (Fanetti *et al.*, 2014).

re-association (Fig. 3). However, Ganymede (Vance *et al.*, 2014; Saur *et al.*, 2015) and Saturn's moon Titan (Grasset and Pargamin, 2005; Tobie *et al.*, 2012) likely possess deep subsurface oceans with substantial portions of the liquid water column in the LDW-HDW transition region (Fig. 3). Deep ocean waters of Pluto, and an at least partly differentiated Callisto, would also exceed 0.2 GPa (Spohn and Schubert, 2003; Kuskov and Kronrod, 2005; Hammond *et al.*, 2016). As in Europa, the existence of a thick saline subsurface ocean in Callisto is indicated by a conductive layer at a depth of less than about 300 km inferred from magnetic field perturbations observed by the Galileo spacecraft (Zimmer *et al.*, 2000).

In this context, our finding of increasing ion association with pressure is important for understanding the coupled evolution of ocean salinity and the silicate interiors of the icy satellites. The salts of planetary oceans are acquired chiefly from sub-seafloor weathering reactions (Zolotov and Shock, 2001). About 75 % of the salts produced by low-temperature aqueous alteration of chondrite under oxidising conditions are magnesium sulphate hydrates (Hogenboom *et al.*, 1995). Thus, H_2O + $MgSO_4$ is one of the most relevant model systems for planetary oceans. Consumption of ions by ion pair formation via

$$Mg^{2+} + SO_4^{2-} = MgSO_4^0 \qquad \text{Eq. 1}$$

requires commensurate forward progress of any magnesium silicate weathering reactions, such as olivine:

$$Mg_2SiO_4 + 2H^+ = Mg^{2+} + 2SiO_2 + 2H_2O \qquad \text{Eq. 2}$$

Therefore, the greater extent of salt association in HDW pore waters beneath the ocean floors of large icy satellites will enhance the progress of dissolution reactions relative to expectations based on LDW. This will generate a more voluminous planetary reservoir of altered rock, and – when the pore fluids decompress upon delivery to the oceans – higher ocean salinities. A thick layer of high-pressure ices and hydrates on the floor of a deep cold subsurface ocean (Fig. 3) could decrease this effect, but dissolved salts would diminish such a layer. Ganymede might have a stack of several ocean layers separated by different phases of ice, with the lowest liquid layer adjacent to the rocky mantle below (Vance *et al.*, 2014).

Acknowledgements

This research was supported by the former GFZ visitors program and NSF EAR 1347987 to CEM.

Editor: Wendy Mao

Additional Information

Supplementary Information accompanies this letter at www.geochemicalperspectivesletters.org/article1707

Reprints and permission information is available online at http://www.geochemicalperspectivesletters.org/copyright-and-permissions

Cite this letter as: Schmidt, C., Manning, C.E. (2017) Pressure-induced ion pairing in $MgSO_4$ solutions: Implications for the oceans of icy worlds. *Geochem. Persp. Let.* 3, 66-74.

References

Chatterjee, R.M., Adams, W.A., Davis, A.R. (1974) A high-pressure laser Raman spectroscopic investigation of aqueous magnesium sulfate solutions. *Journal of Physical Chemistry* 78, 246–250.

Fanetti, S., Lapini, A., Paglai, M., Citroni, M., Di Donato, M., Scandolo, S., Righini, R., Bini, R. (2014) Structure and dynamics of low-density and high-density liquid water at high pressure. *Journal of Physical Chemistry Letters* 5, 235–240.

Fernandez, D.P., Mulev, Y., Goodwin, A.R.H., Levelt Sengers, J.M.H. (1995) A database for the static dielectric constant of water and steam. *Journal of Physical and Chemical Reference Data* 24, 33–53.

Grasset, O., Pargamin, J. (2005) The ammonia-water system at high pressures: Implications for the methane of Titan. *Planetary and Space Science* 53, 371–384.

Hammond, N.P., Barr, A.C., Parmentier, E.M. (2016) Recent tectonic activity on Pluto driven by phase changes in the ice shell. *Geophysical Research Letters* 43, 6775–6782.

Hand, K.P., Chyba, C.F. (2007) Empirical constraints on the salinity of the Europan ocean and implications for a thin ice shell. *Icarus* 189, 424–438.

Helgeson, H.C., Kirkham, D.H., Flowers, G.C. (1981) Theoretical prediction of the thermodynamic behavior of aqueous electrolytes at high pressures and temperatures. IV. Calculation of activity coefficients, osmotic coefficients, and apparent molal and standard and relative partial molal properties to 5 kb and 600 °C. *American Journal of Science* 281, 1241–1516.

Hogenboom, D.L., Kargel, J.S., Ganasan, J.P., Lee, L. (1995) Magnesium sulfate-water to 400 MPa using a novel piezometer: densities, phase-equilibria, and planetological implications. *Icarus* 115, 258–277.

Kaltenegger, L., Sasselov, D., Rugheimer, S. (2013) Water-planets in the habitable zone: Atmospheric chemistry, observable features, and the case of Kepler-62e and -62f. *Astrophysical Journal Letters* 775, L47.

Kawamoto, T., Ochiai, S., Kagi, H. (2004) Changes in the structure of water deduced from the pressure dependence of the Raman OH frequency. *Journal of Chemical Physics* 120, 5867–5870.

Krisch, M., Loubeyre, P., Ruocco, G., Sette, F., Cunsolo, A., D'Astuto, M., LeToullec, R., Lorenzen, M., Mermet, A., Monaco, G., Verbeni, R. (2002) Pressure evolution of the high-frequency sound velocity in liquid water. *Physical Review Letters* 89, 125502.

Kuskov, O.L., Kronrod, V.A. (2005) Internal structure of Europa and Callisto. *Icarus* 177, 550–569.

Li, F., Cui, C.L., He, Z., Cui, T., Zhang, J., Zhou, Q., Zou, G.T., Sasaki, S. (2005) High pressure-temperature Brillouin study of liquid water: Evidence of the structural transition from low-density water to high-density water. *Journal of Chemical Physics* 123, 174511.

Marcus, Y. (2009) Effect of ions on the structure of water. *Chemical Reviews* 109, 1346–1370.

Mirwald, P. (2005) Evidence of PVT anomaly boundaries of water at high pressure from compression and $NaCl{\cdot}2H_2O$ dehydration experiments. *Journal of Chemical Physics* 123, 124715.

Okhulkov, A.V., Demianets, Y.N., Gorbaty, Y.E. (1994) X-ray scattering in liquid water at pressures of up to 7.7 kbar: Test of a fluctuation model. *Journal of Chemical Physics* 100, 1578–1588.

Ritzert, G., Franck, E.U. (1968) Electrical conductivity of aqueous solutions at high temperatures and pressures. 1. KCl, $BaCl_2$, $Ba(OH)_2$ and $MgSO_4$ up to 750 °C and 6 kbar. *Berichte der Bunsengesellschaft für physikalische Chemie* 72, 798–808.

Rudolph, W.W., Irmer, G., Hefter, G.T. (2003) Raman spectroscopic investigation of speciation in $MgSO_{4(aq)}$. *Physical Chemistry Chemical Physics* 5, 5253–5261.

Sahle, C., Sternemann, C., Schmidt, C., Lehtola, S., Jahn, S., Simonelli, L., Huotari, S., Hakala, M., Pylkkänen, T., Nyrow, A., Mende, K., Tolan, M., Hämäläinen, K., Wilke, M. (2013) Microscopic structure of water at elevated pressures and temperatures. *Proceedings of the National Academy of Sciences of the United States of America* 110, 6301–6306.

Saur, J., Duling, S., Roth, L., Jia, X., Strobel, D.F., Feldman, P.D., Christensen, U.R., Retherford, K.D., McGrath, M.A., Musacchio, F., Wennmacher, A., Neubauer, F.M., Simon, S., Hartkorn, O. (2015) The search for a subsurface ocean in Ganymede with Hubble Space Telescope observations of its auroral ovals. *Journal of Geophysical Research* 120, 1715–1737.

Schmidt, C. (2009) Raman spectroscopic study of a $H_2O + Na_2SO_4$ solution at 21–600 °C and 0.1 MPa to 1.1 GPa: Relative differential ν_1-SO_4^{2-} Raman scattering cross sections and evidence of the liquid–liquid transition. *Geochimica et Cosmochimica Acta* 73, 425–437.

Soper, A.K., Ricci, M.A. (2000) Structures of high-density and low-density water. *Physical Review Letters* 84, 2881–2884.

Spohn, T., Schubert, G. (2003) Oceans in the icy Galilean satellites of Jupiter? *Icarus* 161, 456–467.

Sverjensky, D.A., Harrison, B., Azzolini, D. (2014) Water in the deep Earth: The dielectric constant and the solubilities of quartz and corundum to 60 kb and 1200 °C. *Geochimica et Cosmochimica Acta* 129, 125–145.

Tobie, G., Gautier, D., Hersant, F. (2012) Titan's bulk composition constrained by Cassini-Huygens: implication for internal outgassing. *Astrophysical Journal* 752, 125.

Valenti, P., Bodnar, R.J., Schmidt, C. (2012) Experimental determination of H_2O–NaCl liquidi to 25 mass% NaCl and 1.4 GPa: Application to the Jovian satellite Europa. *Geochimica et Cosmochimica Acta* 92, 117–128.

Vance, S., Bouffard, M., Choukroun, M., Sotin, C. (2014) Ganymede's internal structure including thermodynamics of magnesium sulfate oceans in contact with ice. *Planetary and Space Science* 96, 62–70.

Walrafen, G.E. (1962) Raman spectral studies of the effects of electrolytes on water structure. *Journal of Chemical Physics* 36, 1035–1042.

Zimmer, C., Khurana, K.K., Kivelson, M.G. (2000) Subsurface oceans on Europa and Callisto: Constraints from Galileo magnetometer observations. *Icarus* 147, 329–347.

Zolotov, M.Y., Shock, E.L. (2001) Composition and stability of salts on the surface of Europa and their oceanic origin. *Journal of Geophysical Research* 106, 32815–32827.

Pressure-induced ion pairing in $MgSO_4$ solutions: Implications for the oceans of icy worlds

C. Schmidt[1]*, C.E. Manning[2]

Supplementary Information

The Supplementary Information includes:

- Methods
- Discussion of Validity of Results
- Discussion of Results at 50 to 150 °C
- Supplementary Information References

Methods

An externally heated Bassett-type HDAC (Bassett *et al.*, 1993) equipped with type Ia ultra-low fluorescence and ultra-low birefringence diamond anvils (culet diameter 0.9 mm) was used for all experiments. The temperature in the sample chamber of the cell was measured using K-type thermocouples attached to the diamonds. Temperature was calibrated by measurement of two phase-transition temperatures, water ice melting in presence of liquid and vapour (triple point at 0.01 °C and 0.6 kPa) and the transformation from α-quartz to β-quartz (574 °C at 0.1 MPa). Accuracy and reproducibility of the temperature measurements were about ±0.1 °C between -5 and 0 °C (for measurement of the vapour-saturated liquidus temperature of the $MgSO_4$ solution in the sample chamber) and about ±0.5 °C for experiments at 50 to 150 °C. The power input to the resistive heaters was controlled using Eurotherm® 2408 temperature controllers, which held the set temperature within ±0.2 °C during acquisition of Raman spectra. A set of $MgSO_4$ solutions of varying composition was prepared from chromatographic grade H_2O (LiChrosolv®, Merck) and analytic grade magnesium sulphate

1. Deutsches GeoForschungsZentrum (GFZ), Section 4.3 Chemistry and Physics of Earth Materials, Telegrafenberg, 14473 Potsdam, Germany
* Corresponding author (email: Christian.Schmidt@gfz-potsdam.de)
2. Department of Earth, Planetary, and Space Sciences, University of California, Los Angeles, CA 90025-1567, USA

heptahydrate (Merck). For a given experimental series, a piece of natural quartz was loaded with a drop of solution into the HDAC sample chamber formed by a hole with a diameter of 300 or 400 µm in a rhenium gasket separating the anvils. To minimise background fluorescence, care was taken during preparation and loading to avoid contamination by organic materials, particularly by residue made by fingers touching a surface. The procedure for loading and sealing the sample chamber led to minor but unavoidable H_2O evaporation, so the $MgSO_4$ concentration in the solution composition needed to be re-determined. This was done by measurement of the vapour-saturated liquidus temperature (cryometry). First, prior to sealing, an air bubble was allowed to grow to about 10 % of the liquid volume by controlled leaking of the chamber. The sample chamber was then sealed by slight compression of the gasket between the anvils, and the sample was frozen. The ice or $MgSO_4$ hydrate melting temperature in the presence of vapour was then determined, giving the $MgSO_4$ concentration from comparison to literature data (Wolf, 1966; Hogenboom *et al.*, 1995; Marion and Farren, 1999). Magnesium sulphate concentrations determined by cryometry were checked by comparison with concentrations calculated from the full width at half maximum of the fitted SO_4* component of the ν_1-SO_4^{2-} Raman band (Fig. S-1a), calibrated using $MgSO_4$ standard solutions in glass containers. The results from both techniques were in very good agreement. The error in the reported $MgSO_4$ concentrations is ±0.05 molal. For $MgSO_4$ concentrations of 0.5, 1.7, and 2.0 molal, the experiments were performed along the 21 °C isotherm with stepwise increase of the pressure by compression of the sample chamber until solids formed. At each pressure step, Raman spectra of the fluid were collected in the region of the ν_1-SO_4^{2-} mode and additionally in the region of the O–H stretching vibrations of water in the 2.0 molal $MgSO_4$ experiments. In the runs along the 21 °C isotherm, the pressure was determined by recording Raman spectra of quartz before and after those of the aqueous solution and using the calibrated frequency shift of the 206 cm^{-1} Raman line of quartz and equation 5 in Schmidt and Ziemann (2000). Two additional experimental series were performed on 0.75 and 2.25 molal $MgSO_4$ solutions along several isochoric or quasi-isochoric paths at 50, 75, 100, 125, and 150 °C. In these runs, pressures above the vapour pressures of the solutions were obtained from the calibrated frequency shift of the 464 cm^{-1} Raman line of quartz using the equations 2 and 3 in Schmidt and Ziemann (2000). The random error in the obtained pressures was about 10 MPa if the 206 cm^{-1} Raman line of quartz was used, or about 25 MPa in the case of the 464 cm^{-1} line. The experiments at elevated temperatures were restricted to $T \leq 150$ °C to avoid precipitation of kieserite ($MgSO_4 \cdot H_2O$) (Hogenboom *et al.*, 1995; Jahn and Schmidt, 2010) and liquid-liquid phase separation (Wang *et al.*, 2013), and terminated upon gasket failure. The unpolarised Raman spectra of solutions and quartz were acquired using a HORIBA Jobin Yvon LabRAM HR800 UV-Vis Raman microprobe (gratings 1800 lines/mm, focal length 800 mm) equipped with a thermoelectrically cooled CCD-detector (1024 × 256 pixel). The spectra were obtained in backscattering geometry with a Nikon MPlan SLWD 40× objective (numerical aperture 0.4), a confocal pinhole aperture of 100 µm, and using the 488.0 nm argon ion laser line for excitation. The laser interference filter was

removed to record plasma lines from the Ar^+ laser and the Raman lines in the same spectrum. The frequency shift of the quartz lines was calibrated using the plasma lines at 221.54, 351.60, and 520.30 cm^{-1} and the frequencies of the ν_1-SO_4^{2-} band components by monitoring the plasma lines at 737.28 and 1056.94 cm^{-1}. The laser power was set to 275 mW at the source, which was low enough to avoid laser heating of the sample in the HDAC (Schmidt, 2009). Raman spectra of the solutions were collected with 20 accumulations of 5 s each to minimise spectral noise and to attain low and linear backgrounds of similar intensity. Before acquisition of these spectra, the nominal focal point position was always set to 20 µm below upper sample chamber surface to obtain comparable integrated intensities of the Raman bands (Everall, 2000; Schmidt and Chou, 2012). Spectral fitting was done using the software package PeakFit v4.11 from SYSTAT Software Inc., a linear baseline, and the Gaussian-Lorentzian sum (area) function with the same shape factor (*i.e.* the same degree of Lorentzian character) for all peaks in an individual fit of the two ν_1-SO_4^{2-} components (Rudolph *et al.*, 2003) and the three components in the O-H stretching region of water (Brubach *et al.*, 2005). The Pearson IV model was used for the Raman lines of quartz and the plasma lines to allow for peak asymmetry (Schmidt and Ziemann, 2000; Schmidt, 2009). This procedure resulted in a very good description of the shape of the recorded Raman bands, *i.e.* non-statistical residuals were insignificant in all cases. The signal-to-noise ratio in the Raman spectra did not permit reliable fitting of additional components in the O–H stretching region with consistent results.

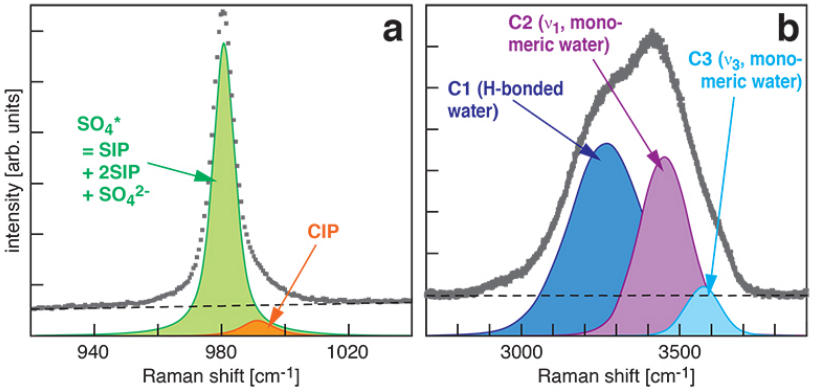

Figure S-1 Raman spectra of a 2.0 molal $MgSO_4$ solution at 21 °C, 0.1 MPa. The fitted baselines are shown as dashed lines. **(a)** ν_1-SO_4^{2-} region, with two fitted band components assigned to CIP (contact ion pairs) and SO_4* (including solvent-separated ion pairs (SIP, 2SIP) and unassociated SO_4^{2-} ions). **(b)** O–H stretching region, with three fitted band components, C1 (mostly from hydrogen-bonded water), C2 (assigned to the symmetric stretching vibration, ν_1, of H_2O monomers), and C3 (assigned to the antisymmetric stretching vibration, ν_3, of H_2O monomers).

Discussion of Validity of Results

Our observations point to a previously unrecognised tendency for progressively increasing contact ion pairing with rising pressure in high-density water at ambient temperature. Alternative explanations are not viable. The internal consistency of all collected data at three concentrations argues strongly against an artefact from hypothetical water loss during the experiments and against any non-isoplethic behaviour. Dissolved silica or rhenium can likewise be excluded as causes because the solubilities of Re and quartz (Manning, 1994; Xiong and Wood, 1999) are many orders of magnitude lower than the magnesium sulphate concentration at all pressure-temperature conditions of this study, and no rhenium or other sulphate was observed to form in the sample chamber. An artefact due to variable and nonlinear background can be excluded because all spectra were fitted using the same procedure and had low and very near linear backgrounds in the frequency region of the ν_1-SO_4^{2-} Raman mode. The fluorescence contribution from the solution or the diamond anvils was insignificant. Fitting of spectra in which the measured background of the diamond anvil was subtracted from the spectrum of the solution yielded results that were almost identical. The enhanced contact ion-pairing shown in Figure 1 could have been the result of an increase in temperature by about 10 to 15 °C during isothermal compression, but monitored temperature changes were <1 °C. Laser heating could have increased the percentage of CIP, but the determined fractions of CIP in the solutions in the HDAC at 0.1 MPa are even slightly lower than literature data (Rudolph *et al.*, 2003) from Raman spectra acquired at much higher laser power at the sample. Finally, significantly different pressure dependencies of the ν_1-SO_4^{2-} Raman scattering cross sections of CIP and SO_4* are implausible because they stem from the same vibrational mode of SO_4^{2-}. Furthermore, this would be in conflict with the fact that equal Raman scattering coefficients of CIP and SO_4* at ~25 °C, 0.1 MPa are verified by the close agreement of Raman spectroscopic speciation data for $MgSO_4$ solutions with data from electrical conductivity measurements and dielectric relaxation and ultrasound absorption spectroscopy (Fisher, 1962; Davis and Oliver, 1973; Rull *et al.*, 1994; Tomšič *et al.*, 2002; Rudolph *et al.*, 2003; Buchner *et al.*, 2004; Akilan *et al.*, 2006).

Discussion of Results at 50 to 150 °C

For 0.75 and 2.25 molal $MgSO_4$ solutions, we determined the variation in the percentage of $Mg^{2+}SO_4^{2-}$(aq) contact ion pairs with pressure at 50, 75, 100, 125, and 150 °C (Fig. S-2). The percentage of CIP generally decreased with pressure along these isotherms. Although the slopes become considerably less negative with pressure, there is no clear evidence for increasing ion association for any isotherm. If our observation of pressure-induced salt association is related to the LDW-HDW transition, then the high temperature data imply that HDW stability either disappears with increasing temperature or moves rapidly to high pressure. Raman, infrared, and Brillouin spectroscopic studies show that the LDW-HDW transition becomes increasingly difficult to detect above ambient temperature,

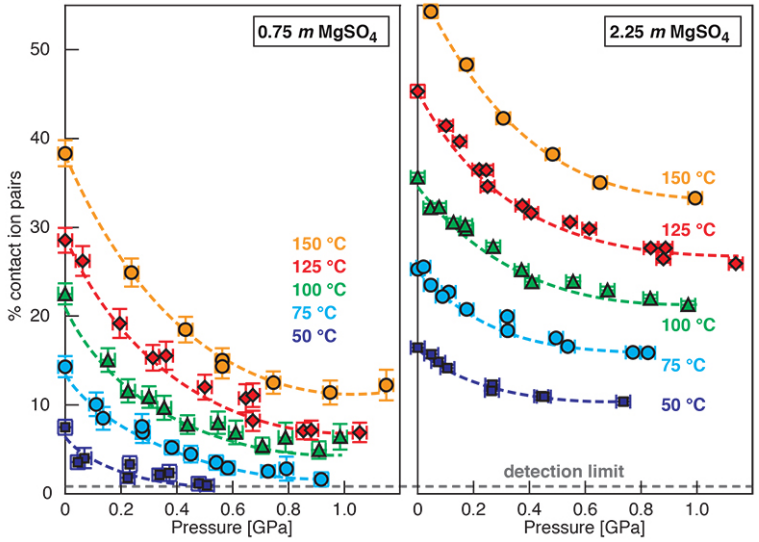

Figure S-2 Percentage of contact ion pairs in 0.75 and 2.25 molal $MgSO_4$ solutions as a function of pressure along isotherms (dark blue, 50 °C; cyan, 75 °C; green, 100 °C; red, 125 °C; orange, 150 °C). Vertical error bars, 2 standard errors; horizontal error bars, uncertainty in the pressure obtained from the shift in the wavenumber of the 464 cm^{-1} Raman line of quartz.

even at 50 °C (Li *et al.*, 2005; Okada *et al.*, 2005; Schmidt, 2009; Fanetti *et al.*, 2014b). There is no consensus on the ∂P/∂T slope of the LDW-HDW transition. The available experimental constraints variously suggest slopes that are strongly positive (0.4 ± 0.1 GPa at 25 °C, 1.0 ± 0.1 GPa at 100 °C, and 1.3 ± 0.1 GPa at 300 °C) (Kawamoto *et al.*, 2004), to slightly negative (0.29 GPa at 293 K, 0.21 GPa at 316 K, and 0.19 GPa at 353 K) (Li *et al.*, 2005), to negative (~0.2 GPa at 273.7 K, ~0.16 GPa at 298.0 K, ~0.11 GPa at 318.0 K, and ~0.08 GPa at 339.0 K) with the interpretation that LDW ceases to exist at ~363 K (Fanetti *et al.*, 2014b). Although the most recent data of Fanetti *et al.*, (2014b) appear to be of high quality, it should be noted that the implied change in the solvent structure at ~363 K would affect volume and entropy of reactions. However, to our knowledge, there are no anomalies in vapour pressure or aqueous solubility curves at about this temperature. At lower temperatures, anomalies in reaction curves exist at pressures near the LDW transition, *e.g.*, a change from a negative to a positive ∂P/∂T slope of the hydrohalite liquidus at -7.5 °C and 140 ± 40 MPa (Valenti *et al.*, 2013) and an inflection in the dehydration curve of $NaCl{\cdot}2H_2O$ at 12 °C, 0.27 GPa (Mirwald, 2005). Moreover, the minimum in the isothermal compressibility of water is at 46.5 °C. Above this temperature, water behaves like a regular liquid, which would be incompatible with a transition from more compressible LDW to less compressible HDW (Li *et al.*, 2005) at about 90 °C. Furthermore, for the ν_1-SO_4^{2-} Raman band of a 1.54 molal Na_2SO_4 solution, the slopes of the wavenumber with

pressure at 100, 200, 300, 400, and 500 °C are similar to that of LDW at 21 °C, and the slopes of the line width with pressure at 100, 200, 300, 400, and 500 °C are much closer to that of LDW than that of HDW at 21 °C (Schmidt, 2009). In summary, the considerations above are consistent with our interpretation that a relationship exists between ion paring behaviour and the LDW-HDW transition, and that this behaviour is a low-temperature phenomenon.

Supplementary Information References

Akilan, C., Rohman, N., Hefter, G., Buchner, R. (2006) Temperature effects on ion association and hydration in $MgSO_4$ by dielectric spectroscopy. *ChemPhysChem* 7, 2319–2330.

Bassett, W.A., Shen, A.H., Bucknum, M., Chou I-M. (1993) A new diamond anvil cell for hydrothermal studies to 10 GPa and -190 °C to 1100 °C. *Review of Scientific Instruments* 64, 2340–2345.

Brubach, J.B., Mermet, A., Filabozzi, A., Gerschel, A., Roy, P. (2005) Signatures of the hydrogen bonding in the infrared bands of water. *Journal of Chemical Physics* 1022, 184509.

Buchner, R., Chen, T., Hefter, G. (2004) Complexity in "simple" electrolyte solutions: ion pairing in $MgSO_{4(aq)}$. *Journal of Physical Chemistry B* 108, 2365–2375.

Davis, A.R., Oliver, B.G. (1973) Raman spectroscopic evidence for contact ion pairing in aqueous magnesium sulfate solutions. *Journal of Physical Chemistry* 77, 1315–1316.

Everall, N.J. (2000) Confocal Raman microscopy: why the depth resolution and spatial accuracy can be much worse than you think. *Applied Spectroscopy* 54, 773–782.

Fanetti, S., Paglai, M., Citroni, M., Lapini, A., Scandolo, S., Righini, R., Bini, R. (2014b) Connecting the water phase diagram to the metastable domain: High-pressure studies in the supercooled regime. *Journal of Physical Chemistry Letters* 5, 3804–3809.

Fisher, F.H. (1962) The effect of pressure on the equilibrium of magnesium sulfate. *Journal of Physical Chemistry* 66, 1607–1611.

Hogenboom, D.L., Kargel, J.S., Ganasan, J.P., Lee, L. (1995) Magnesium sulfate-water to 400 MPa using a novel piezometer: densities, phase-equilibria, and planetological implications. *Icarus* 115, 258–277.

Jahn, S., Schmidt, C. (2010) Speciation in aqueous $MgSO_4$ fluids at high pressures and high temperatures from ab initio molecular dynamics and Raman spectroscopy. *Journal of Physical Chemistry B* 114, 15565–15572.

Kawamoto, T., Ochiai, S., Kagi, H. (2004) Changes in the structure of water deduced from the pressure dependence of the Raman OH frequency. *Journal of Chemical Physics* 120, 5867–5870.

Li, F., Cui, C.L., He, Z., Cui, T., Zhang, J., Zhou, Q., Zou, G.T., Sasaki, S. (2005) High pressure-temperature Brillouin study of liquid water: Evidence of the structural transition from low-density water to high-density water. *Journal of Chemical Physics* 123, 174511.

Manning, C.E. (1994) The solubility of quartz in H_2O in the lower crust and upper mantle. *Geochimica et Cosmochimica Acta* 58, 4831–4839.

Marion, G.M., Farren, R.E. (1999) Mineral solubilities in the Na-K-Mg-Ca-Cl-SO_4-H_2O system: A re-evaluation of the sulfate chemistry in the Spencer-Møller-Weare model. *Geochimica et Cosmochimica Acta* 63, 1305–1318.

Mirwald, P. (2005) Evidence of PVT anomaly boundaries of water at high pressure from compression and $NaCl{\cdot}2H_2O$ dehydration experiments. *Journal of Chemical Physics* 123, 124715.

Okada, T., Komatsu, K., Kawamoto, T., Yamanaka, T., Kagi, H. (2005) Pressure response of Raman spectra of water and its implication to the change in hydrogen bond interaction. *Spectrochimica Acta Part A* 61, 2423–2427.

Rudolph, W.W., Irmer, G., Hefter, G.T. (2003) Raman spectroscopic investigation of speciation in $MgSO_{4(aq)}$. *Physical Chemistry Chemical Physics* 5, 5253–5261.

Rull, F., Balarew, C., Alvarez, J.L., Sobron, F., Rodriguez, A. (1994) Raman spectroscopic study of ion association in aqueous magnesium-sulfate solutions. *Journal of Raman Spectroscopy* 25, 933–941.

Schmidt, C. (2009) Raman spectroscopic study of a H_2O + Na_2SO_4 solution at 21–600 °C and 0.1 MPa to 1.1 GPa: Relative differential $\nu1$-SO_4^{2-} Raman scattering cross sections and evidence of the liquid–liquid transition. *Geochimica et Cosmochimica Acta* 73, 425–437.

Schmidt, C., Ziemann, M.A. (2000) In-situ Raman spectroscopy of quartz: A pressure sensor for hydrothermal diamond-anvil cell experiments at elevated temperatures. *American Mineralogist* 85, 1725–1734.

Schmidt, C., Chou, I-M. (2012) The hydrothermal diamond anvil cell (HDAC) for Raman spectroscopic studies of geological fluids at high pressures and temperatures. In: Dubessy, J., Caumon, M.-C., Rull, F. (Eds.) *Raman Spectroscopy applied to Earth Sciences and Cultural Heritage*. EMU Notes in Mineralogy, Vol. 12, 247–276.

Tomšič, M., Bester-Rogač, M., Jamnik, A., Neueder, R., Barthel, J. (2002) Conductivity of magnesium sulfate in water from 5 to 35 °C and from infinite dilution to saturation. *Journal of Solution Chemistry* 31, 19–31.

Valenti, P., Bodnar, R.J., Schmidt, C. (2012) Experimental determination of H_2O–NaCl liquidi to 25 mass% NaCl and 1.4 GPa: Application to the Jovian satellite Europa. *Geochimica et Cosmochimica Acta* 92, 117–128.

Wang, X., Chou, I-M., Hu, W., Burruss, R.C. (2013) *In-situ* observations of liquid-liquid phase separation in aqueous $MgSO_4$ solutions: Geological and geochemical implications. *Geochimica et Cosmochimica Acta* 103, 1–10.

Wolf, A.V. (1966) *Aqueous solutions and body fluids: their concentrative properties and conversion tables*. Harper & Row, New York.

Xiong, Y., Wood, S.A. (1999) Experimental determination of the solubility of ReO_2 and the dominant oxidation state of rhenium in hydrothermal solutions. *Chemical Geology* 158, 245–256.